SPECIAL REPORT

Combining electrophysiological and hemodynamic measures of the auditory oddball

B. OPITZ, A. MECKLINGER, D.Y. VON CRAMON, AND F. KRUGGEL

Max-Planck-Institute of Cognitive Neuroscience, Leipzig, Germany

Abstract

The neural mechanisms of deviancy and target detection were investigated by combining high density event-related potential (ERP) recordings with functional magnetic resonance imaging (fMRI). ERP and fMRI responses were recorded using the same paradigm and the same subjects. Unattended deviants elicited a mismatch negativity (MMN) in the ERP. In the fMRI data, activations of transverse/superior temporal gyri bilateral were found. Attended deviants generated an MMN followed by an N2/P3b complex. For this condition, fMRI activations in both superior temporal gyri and the neostriatum were found. These activations were taken as neuroanatomical constraints for the localization of equivalent current dipoles. Inverse solutions for dipole orientation provide evidence for significant activation close to Heschl's gyri during deviancy processing in the 110–160-ms time interval (MMN), whereas target detection could be modeled by two dipoles in the superior temporal gyrus between 320 and 380 ms.

Descriptors: ERP, fMRI, Auditory oddball, Mismatch negativity, Target detection

The ability to discriminate and identify events is important for successful interaction with the environment. A special case of discrimination is deviance detection in the auditory modality. According to Schröger (1997), this ability may be based on a detection system that does not rely on attention. An electrophysiological indicator of this preattentive change detection mechanism is the mismatch negativity (MMN), a frontally distributed negative deflection in the event-related brain potential (ERP), peaking between 100–200 ms after stimulus onset.

Most attempts to localize MMN sources are based on dipole analyses of electrical and magnetoencephalographic (MEG) recordings or scalp current density mappings. The main generators of the MMN were estimated in left and right auditory cortices (Alho et al., 1998; Scherg, Vajsar, & Picton, 1989). Additional contributions come from the lateral surface of the temporal lobes (Paavilainen, Alho, Reinikainen, Sams, & Näätänen, 1991) and prefrontal cortical areas (Giard, Perrin, Pernier, & Bouchet, 1990). This prefrontal activity might be generated by mechanisms initiating an involuntary switch of attention towards the stimulus change (Näätänen, 1992). In ERPs to deviant stimuli in an attended auditory stimulus sequence (targets), MMN is followed by a fronto-centrally distributed N2b and a parietally maximal P3b (Näätänen, 1992). Different cortical sources of the P3b component have been suggested. Sources in the temporal cortex and in the medial temporal lobe were suggested based on electrical source analyses (Meck-

linger & Ullsperger, 1995; Tarkka, Stokić, Basile, & Papanicolaou, 1995). In combination with functional magnetic resonance imaging (fMRI), sources in the supramarginal gyrus, thalamus, and anterior cingulate gyrus have been found (Menon, Ford, Lim, Glover, & Pfefferbaum, 1997). Human lesion studies have suggested that the temporoparietal junction might be an important contributor to P3b potentials (Knight, Scabini, Woods, & Clayworth, 1989). Source localization performed on the basis of MEG data suggested contributions from subcortical sources (Meckinger et al., 1998) and temporal cortex (Alho et al., 1998). Large P3b-like responses have also been recorded from other brain structures, including temporal cortex, hippocampus, and thalamus (Halgren et al., 1995). Thus, there is no complete picture regarding the sources of the P3b component because several tasks and various methods with different properties were used. Neuroimaging techniques like fMRI (McCarthy, Luby, Gore, & Goldman-Rakic, 1997) are capable of localizing brain structures underlying specific cognitive functions with a high spatial resolution, but to date the temporal resolution of these methods varies between 2 and 60 s. In contrast, ERPs provide a measure of brain activity related to cognitive functions with millisecond accuracy. The major goal of this study was to investigate the neural circuits underlying deviancy and target detection and the temporal characteristics of brain activation during these processes by combining the superior temporal resolution of ERPs with the high spatial resolution of fMRI.

Materials and Methods

Subjects

Sixteen paid right-handed healthy volunteers (6 men, 10 women; ages 20–28 years, median = 22 years) participated in the experiment.

Stimuli

Pure sine tones with frequencies of 600 Hz and 1000 Hz were used. All stimuli had a duration of 200 ms (including 10-ms rise and 40-ms fall time) and were presented at 75 dB/SPL via speakers (for the electroencephalogram [EEG]) or airconducting headphones (fMRI).

Procedure

Based on ERP studies that have shown that the amplitude and the latency of the MMN component is unaffected by the predictability of deviant stimuli (Scherg et al., 1989), we used a blocked design with alternating standard and deviant blocks. Standard blocks were comprised of 24 low tones, and deviant blocks were comprised of 16 low and 8 high (deviant) tones. The interstimulus interval from offset to onset was 550 ms.

There were two runs of 24 blocks each (12 standard and 12 deviant blocks), yielding a probability of deviants of .33 within a block and .165 across all 24 blocks. During the first run, subjects were required to watch a cartoon video (unattend condition). During the second run they had to fixate the center of the screen and silently count the high tones (attend condition). This task order was kept constant across subjects.

Following this standard oddball task, subjects were presented with two runs of a novelty oddball task (attend vs. unattend). Here, we focus on the standard oddball task. The results of the novelty oddball will be reported elsewhere (Opitz, Mecklinger, Friederici, & von Cramon, 1998).

EEG Recordings

EEG and electrooculogram (EOG) were recorded continuously from 120 electrode sites using an Electrocap. The signals were on-line bandpass filtered (0.1–70 Hz) and digitized at a rate of 250 Hz. Vertical and horizontal EOG were recorded from three electrode pairs placed on the infra- and supraorbital ridges of the left and the right eye and on the outer canthi of the two eyes. All leads were referenced to the nose tip. Electrode impedance was kept below 2 kOhms. ERP data were epoched off-line for an 800-ms period (including a 200-ms prestimulus baseline). Prior to averaging, epochs were scanned for eye movement and other artifacts and were excluded from averaging when the standard deviation exceeded 40 μV. ERPs were computed separately for standard and deviant tones. For analogous comparison to fMRI data, only difference waveforms (deviant minus standard) were analyzed. The latency of ERP components was measured relative to stimulus onset. The component's amplitude was quantified as the mean

Table 1. *fMRI Activation Peaks Associated with Processing of Deviant Stimuli*

Peak location[a]					
x	y	z	p value at peak	Size (mm^3)	Cortical region
−45	−34	13	<.05	178	Left transverse/superior temporal gyrus
44	−31	11	<.05	384	Right transverse/superior temporal gyrus

[a]The x, y, and z coordinates are those of the Talairach and Tournoux (1988) system.

voltage in the 50-ms interval around the peak latency of the respective component, that is, 110–160 ms for the MMN and 330–380 ms for the P3b component. The presence of the MMN was determined by testing its mean amplitude at frontal (Fz) and mastoid (ML) recording sites against zero level with Student's t test.

MRI

High-resolution whole-brain images were acquired to assist localization of activation foci using a T1 weighted 3-D segmented MDEFT. The matrix of $256 \times 256 \times 128$ pixels covered a field of view (FOV) of 250 mm.

fMRI

Functional images were acquired at 3T on a Bruker Medspec 30/100 system using a standard head coil. Cushions served to reduce motion. Gradient echo planar images (TE = 40 ms) were collected from seven axial slices parallel to the AC-PC line at a rate of 2 s per image. Slice thickness was 6 mm, and interslice distance was 2 mm. The FOV was 250 mm with a matrix of 128×64. fMRI data were processed using the BRIAN package (Kruggel, Descombes, & von Cramon, 1998). Movement artefacts were detected by thresholding the foreground (brain) / background intensity ratio for each timestep. Slices at timesteps with this ratio being lower than 12.5 were classified as artifact containing (Kruggel et al., 1998). Because of a large number of artifact-contaminated time steps, two subjects were excluded from fMRI and ERP analyses. Markov random fields, as described in Kruggel et al. (1998), were applied for image restoration. Thus the effect of spatial smoothing was minimal and mainly ensured spatial homogeneity. Voxel-wise Pearson correlations of fMRI time series with a box car reference waveform were calculated to determine activation related to the processing in deviant blocks. The box car function resembled the blocked design and was delayed by 4 s (cf. Buckner, Koutstaal, Schacter, Wagner, & Rosen, 1998) relative to the begining of a block. The correlation statistics were normalized to Z scores. A significance level threshold of $p < .05$ (corrected for multiple spatial comparisons) was used to determine the presence of significant activation foci. Activation maps were registered with individual high-resolution 3-D data sets and transformed into stereotactic Talairach space (Friston et al., 1995). Multisubject averaging was used to enhance the signal-to-noise ratio.
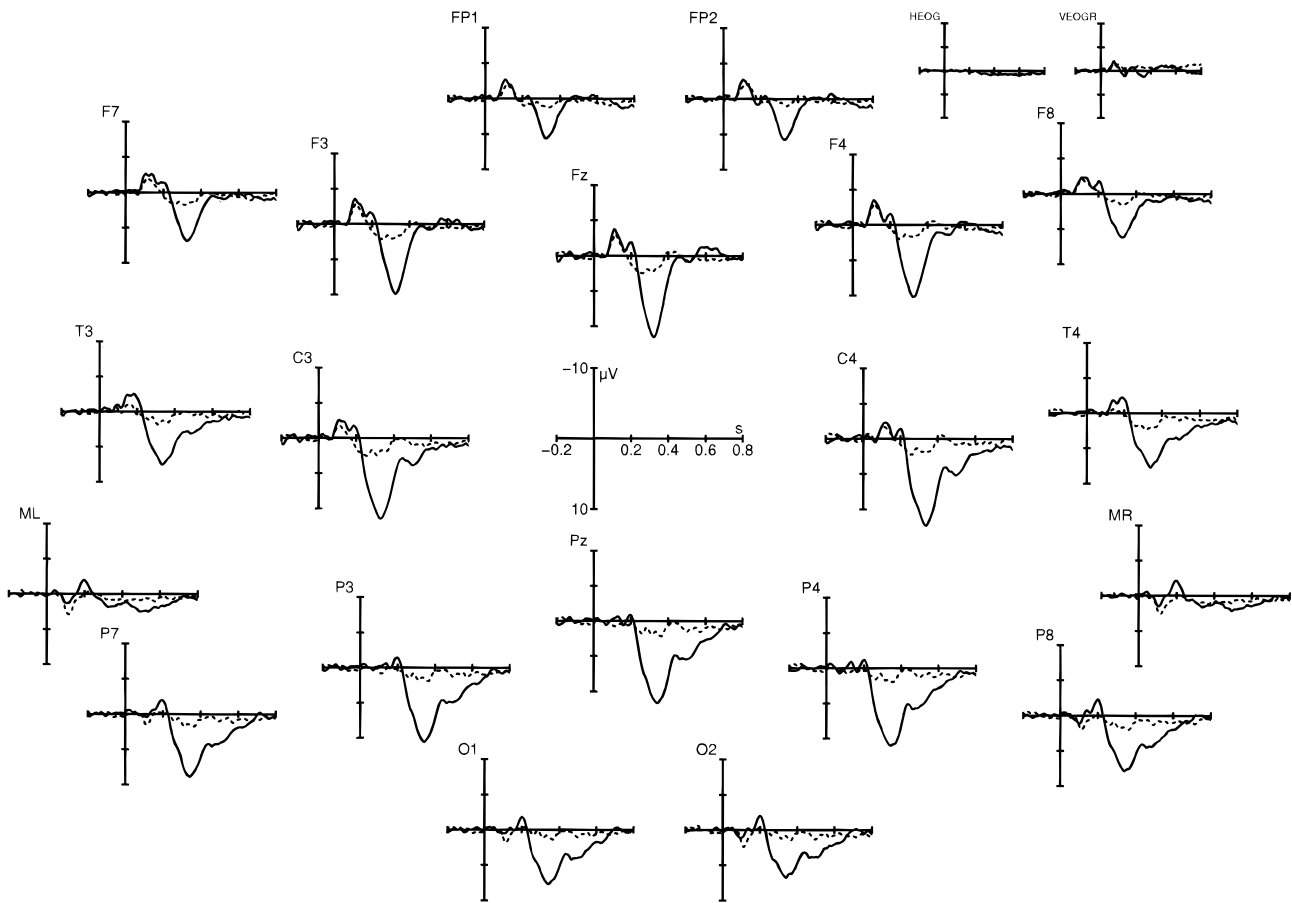
Dipole Modeling

For source localization, realistically shaped head models were developed using the boundary element method. Three compartments of the head were taken into account: the brain (including cerebrospinal fluid), skull, and scalp (Cuffin, 90). The conductivities were set to 0.33 S/m for the brain and scalp and 0.0042 S/m for the skull. The head model was derived from 50 averaged Talairach-normalized MRIs stored in a local brain database.

All estimations related to fMRI or EEG measurements were carried out in a common coordinate system as defined by the nasion and both preauricular points. Dipole locations were kept fixed according to the fMRI activation foci averaged across subjects. Orientations of dipoles were fitted using the average reference ERP data with the ASA software (A.N.T. software BV, Hengelo, The Netherlands). Best-fitting dipole orientations were assumed to be perpendicular to cortical gray matter, in agreement with electrophysiological and anatomical constraints (Nunez, 1990). Goodness of fit was evaluated based on the cross-correlation coefficient between the modeled and the empirical waveforms. Keeping dipole location and orientations fixed, the time course of dipole

Figure 1. Grand average difference waveforms obtained for both conditions by subtracting the ERPs to standard tones from those to deviant tones. Solid line = attend condition; Dashed line = ignore condition. The waveforms are displayed for selected electrodes of the 10–20 system.

strength and the goodness of fit were determined over the period from 100 ms before to 600 ms after stimulus onset.

Results

Unattend Condition

Figure 1 shows the difference waveforms in both the unattend and the attend conditions. In the unattend condition, the deviants elicited a significant MMN component at 128 ms (mean amplitude at Fz -1.8 μV, $t = 3.05$, $p < .01$) with a polarity reversal at mastoid leads (ML 1.7 μV, $t = 5.01$, $p < .001$). The corresponding statistical parametric maps, representing the blood oxygenation level-dependent response to infrequent deviant tones revealed two significant clusters of activity in the left and right transverse temporal gyri (TTG), with the size of this activation being substantially larger in the right TTG (cf. Table 1 for Talairach coordinates and significance). Precise locations of these activation foci superimposed on averaged Talairach-normalized high resolution structural MRIs are shown in Figure 2.

To compare electrophysiological and fMRI data, the scalp ERP distribution was modeled using dipole source locations in both TTG as derived from functional images. The obtained best-fitting orientations were superimposed on the fMRI (Figure 2). The orientations were almost perpendicular to the gray matter. The good-

ness of fit and the time course of the obtained dipole solution are shown in Figure 3. Between 100 and 140 ms, the goodness of fit exceeded 0.95 but it was negligible at points outside this latency window. A similar time course with a peak latency around 120 ms
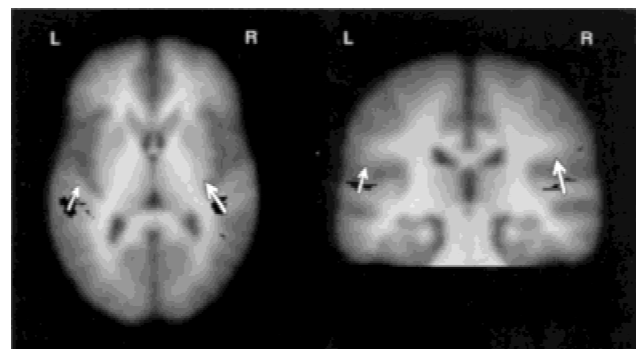
Figure 2. Brain areas that showed significant fMRI activation to deviant stimuli were superimposed on average structural MRI in Talairach space (averaged brain). Best-fitting dipoles are indicated as arrows. The arrow size is proportional to the activation strength within the fit interval (110–160 ms).
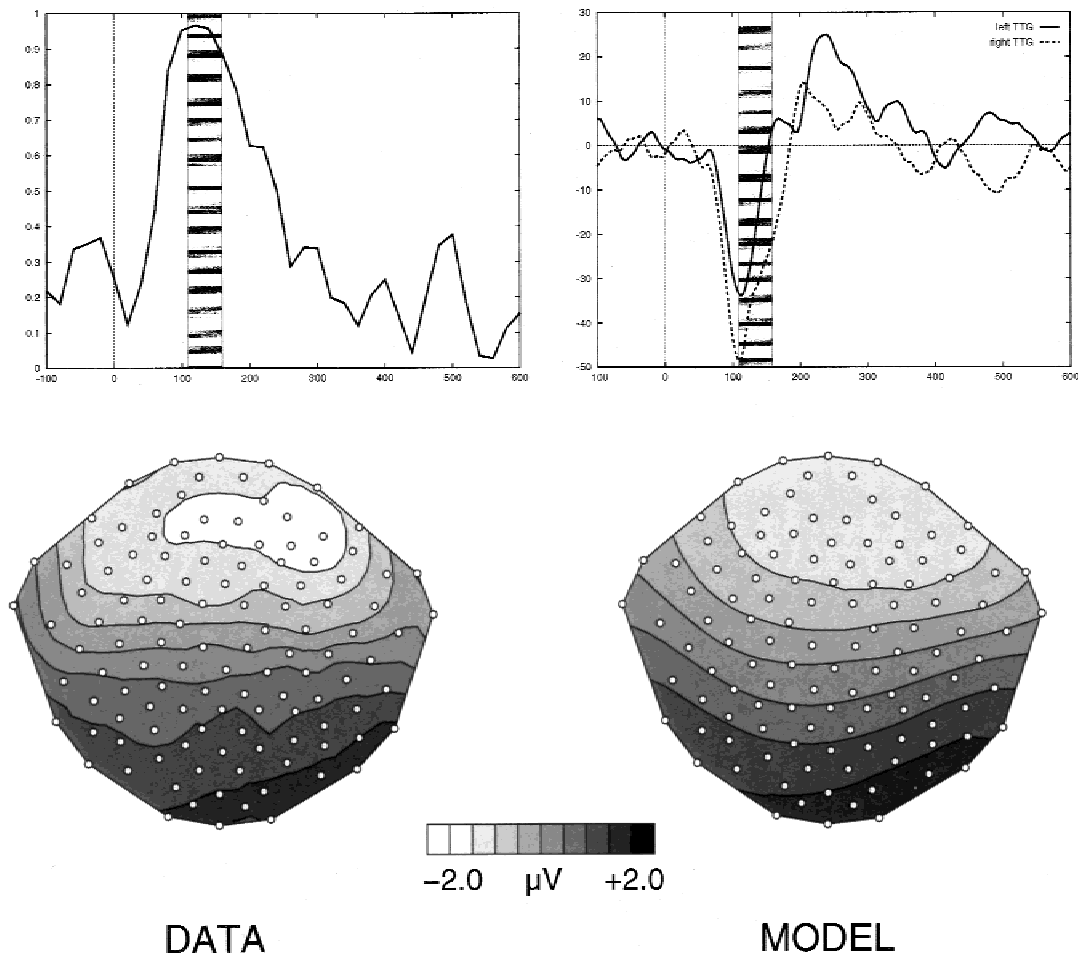
Figure 3. Goodness of fit (% explained variance) as a function of time (upper left panel) and time course (upper right panel) of the obtained dipole model (nAm) of the MMN component. Dipole source locations and orientations were fixed. Gray areas indicate the fit interval. The scalp potential maps for empirical data (left) and the dipole model (right) are shown in the lower part of the figure. TTG = transverse temporal gyrus.

was observed for the activations in both hemispheres (cf. Figure 3). In correspondence to the size of the activation foci obtained in fMRI (cf. Table 1), the dipole in the right hemisphere showed a stronger activation than the left hemisphere dipole (49 nAm vs. 34 nAm at peak).

Attend Condition

Subjects committed less than 2% errors in counting the deviant tones in the attend condition. In this condition, targets evoked a frontally focused MMN (F -2.2 μV, $t = 3.56$, $p < .01$) around 136 ms followed by a N2b/P3b complex (Figure 1). The MMN showed the typical polarity reversal at the left mastoid (ML 0.98 μV, $t = 2.21$, $p < .05$). Targets elicited a parietal maximal P3 component (P3b) with a peak latency of 360 ms at the Pz recording site.

Clusters of activation, related to target processing are displayed in Figure 4. Four significant clusters were obtained with peaks in the posterior part of the left and right superior temporal gyri (STG), adjacent to the supramarginal gyri and the left and right neostriatum. As shown in Table 2, we obtained a right/left asymmetry of activation size in the STG and a reversed laterality pattern in the neostriatum.
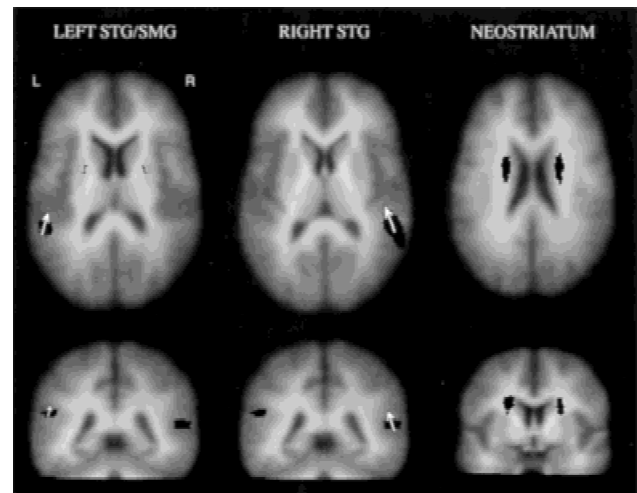
Figure 4. Brain areas that showed significant fMRI activation to target stimuli were superimposed on an averaged brain: left and right superior temporal gyri (STG), left supramarginal gyrus (SMG), and neostriatum. Best-fitting dipoles are indicated as arrows. The arrow size is proportional to the activation strength within the fit interval (330–380 ms).

Table 2. *Brain Areas Significantly Activated During Target Processing*

| Peak location			*p* value at peak	Size (mm^3)	Cortical region
x	*y*	*z*			
47	−41	10	<.01	1,477	Right superior temporal gyrus (posterior part)
−47	−40	18	<.01	785	Left superior temporal gyrus (posterior part)
19	−1	23	<.01	717	Right neostriatum
−19	−5	25	<.001	1,472	Left neostriatum

For modeling the ERP waveforms we first assumed generators at all four locations derived from the fMRI activation pattern. We obtained a stable solution only for dipoles located at both STG. Dipoles located at bilateral neostriatum showed an activation strength of more than 200 nAm unlikely to be explained by neuronal currents (Freeman et al., 1975) and were therefore excluded from the final dipole solution. With dipole source locations fixed in both STG, the best-fitting dipole orientation was determined (cf. Figure 4). The goodness of fit and the activation waveforms of the derived solution are shown in Figure 5. The goodness of fit exceeded 0.95 only within the fitting interval between 340 and 380 ms. The size of fMRI activation foci and the dipole strength again suggest a predominant activation in the right hemisphere.

Discussion

The present study provides electrophysiological and hemodynamic data on the localization of brain activity in an auditory discrimination task. The aim of this study was to combine fMRI and ERP measures to disentangle spatiotemporal characteristics of brain activation underlying deviancy and target detection.

Compared with standard tones, unattended deviant stimuli elicited a frontally distributed MMN component and gave rise to reliable fMRI signal increases in the transverse temporal gyri bilaterally and in the adjacent superior temporal gyri. Inverse source analyses suggested that these temporal regions are the most dominant contributor to the frontally distributed ERPs within
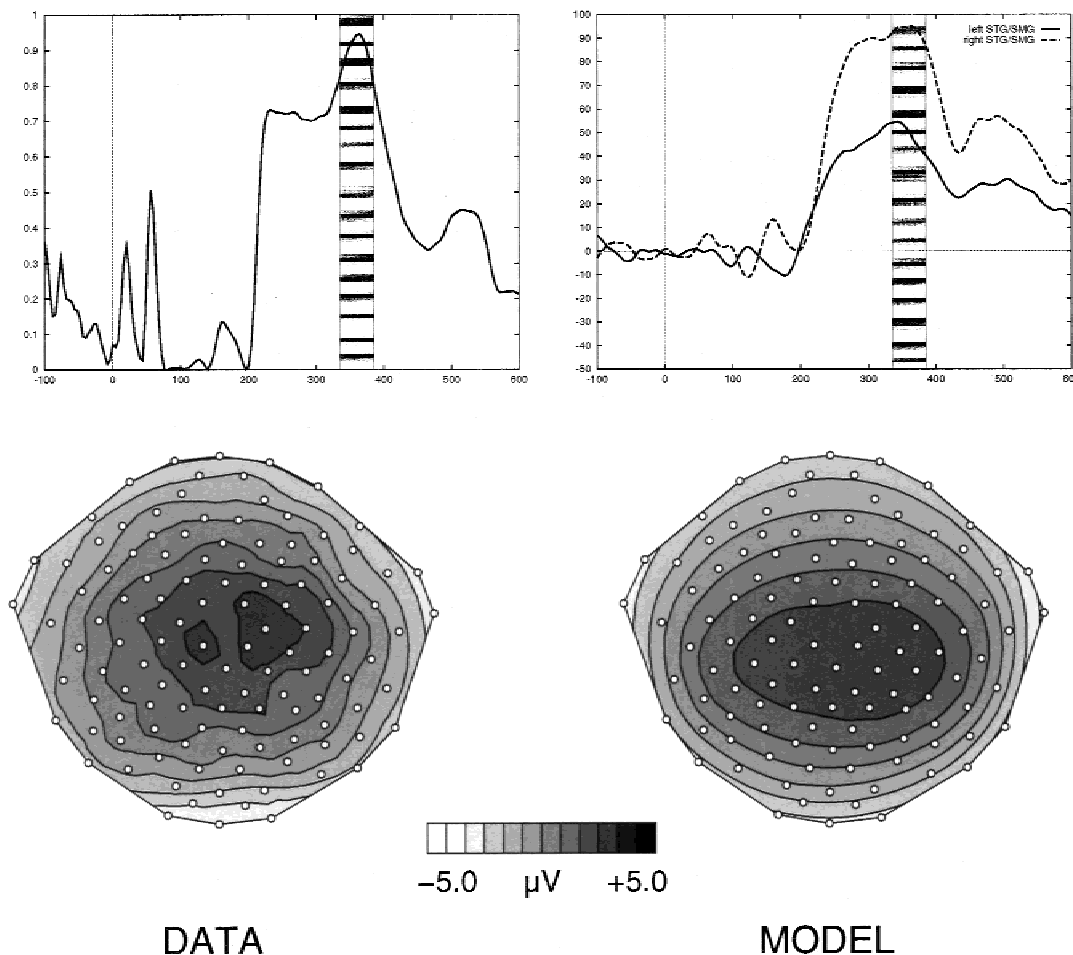
Figure 5. Goodness of fit (% explained variance) as a function of time (upper left panel) and time course of dipole strength (nAm) (upper right panel) and scalp potential maps of the obtained dipole model of the P3b component. Dipole source locations and orientations were kept fixed. Gray areas indicate fit interval. The scalp potential maps of the fit interval for empirical data (left) and the dipole model (right) are shown. STG = superior temporal gyri; SMG = supramarginal gyrus.

the 100–160-ms time window and therefore could account for the generation of the scalp MMN. This suggestion is confirmed by converging results of several studies using different methods (Alho et al., 1998; Halgren et al., 1995; Scherg et al., 1989) showing MMN generators within or in the vicinity of the auditory cortex. However, with the large deviant–standard difference used in this experiment, the waveform in the 110–160-ms interval may also reflect differential refractoriness of the N1 generators of standards and deviants (Scherg et al., 1989). The results suggest that the transverse temporal gyri seem to be involved in automatic change detection processes reflected by the MMN component.

The finding of dominant right hemisphere activation is consistent with the notion of right hemisphere preponderant scalp distribution of the MMN (Näätänen, 1992). The activated area in the right hemisphere may include multiple brain structures. Thus, the right frontal generator suggested by a recent study using scalp current density analyses (Giard et al., 1990) might be partially due to an additional generator located in the right temporal cortex and projecting toward right frontal scalp sites.

The results of the attend condition reveal that the processing of infrequent target stimuli elicited an MMN component followed by an N2b/P3b complex and bilateral fMRI activation foci in the posterior part of the superior temporal cortex and the neostriatum. Inverse source analyses suggest that only the bilateral activation of the posterior part of the superior temporal gyrus contributes to the scalp P3b. This finding is in agreement with intracranial recordings (Halgren et al., 1995) and multimodal neuroimaging techniques (Menon et al., 1997). Recent studies with psychiatric patients showed high correlation of P3 amplitude reduction with volume reductions of gray matter in the left superior temporal gyrus (McCarley, Shenton, O'Donnell, & Faux, 1993).

In addition to the superior temporal gyri, the neostriatum is activated during target detection. Recent studies using single cell recordings in monkeys showed that the majority of responsive neurons in the caudate nucleus and the putamen had activity in relation to stimuli that were dependent on the performance of a task (Rolls, Thorpe, & Maddison, 1983). Thus, at least in some task situations the neostriatum may be part of a neural circuit involved in stimulus–response association. However, further research is required for a more detailed picture of the role of the neostriatum in different task situations.

The present study demonstrates that combined analyses of fMRI and ERP provide a new opportunity for disentangling temporal aspects of neural activation in a distributed network underlying deviancy and target processing.

REFERENCES

Alho, K., Winkler, I., Escera, C., Huotilainen, M., Virtanen, J., Jääskeläinen, I., Pekkonen, E., & Ilmoniemi, R. (1998). Processing of novel sounds and frequency changes in the human auditory cortex: Magneto-encephalographic recordings. *Psychophysiology*, *35*, 211–224.

Buckner, R., Koutstaal, W., Schacter, D., Wagner, A., & Rosen, B. (1998). Functional-anatomic study of episodic retrieval using fMRI: I. Retrieval effort versus retrieval success. *Neuroimage*, *7*, 151–162.

Cuffin, B. (1990). Effects of head shape on EEGs and MEGs. *IEEE Transactions on Biomedical Engineering*, *40*, 44–52.

Freeman, W. (1975). *Action in the nervous system*. New York: Academic Press.

Friston, K., Ashburner, J., Frith, C., Poline, J.-B., Heather, J., & Frackowiak, R. (1995). Spatial registration and normalization of images. *Human Brain Mapping*, *2*, 165–189.

Giard, M., Perrin, F., Pernier, J., & Bouchet, P. (1990). Brain generators implicated in processing of auditory stimulus deviance: A topographic event-related potential study. *Psychophysiology*, *27*, 627–640.

Halgren, E., Baudena, P., Clarke, J., Heit, G., Liegeois, C., & Musolino, A. (1995). Intracerebral potentials to rare target and distractor auditory and visual stimuli. I: Superior temporal and parietal lobe. *Electroencephalography and Clinical Neurophysiology*, *94*, 191–220.

Knight, R., Scabini, D., Woods, D., & Clayworth, C. (1989). Contributions of the temporal–parietal junction to the human auditory P3. *Brain Research*, *502*, 109–116.

Kruggel, F., Descombes, X., & von Cramon, D. (1998). Preprocessing of fMRI datasets. In B. Vemuri (Ed.), *Workshop on biomedical image analysis* (pp. 323–330). Los Angeles: IEEE Press.

McCarley, R., Shenton, M., O'Donnell, B., & Faux, S. (1993). Auditory P300 abnormalities and left posterior superior temporal gyrus volume reduction in schizophrenia. *Archives of General Psychiatry*, *50*, 190–197.

McCarthy, G., Luby, M., Gore, J., & Goldman-Rakic, P. (1997). Infrequent events transiently activate human prefrontal and pareital cortex as measured by functional MRI. *Journal of Neurophysiology*, *77*, 1630–1634.

Mecklinger, A., Maeß, B., Opitz, B., Pfeifer, E., Cheyne, D., & Weinberg, H. (1998). A MEG analysis of the P300 in visual discrimination task. *Electroencephalography and Clinical Neurophysiology*, *108*, 45–56.

Mecklinger, A., & Ullsperger, P. (1995). The P300 to novel and target events: A spatio-temporal dipole model analysis. *Nenroreport*, *7*, 241–245.

Menon, V., Ford, J., Lim, K., Glover, G., & Pfefferbaum, A. (1997). Combined event-related fMRI and EEG evidence for temporal-parietal cortex activation during target detection. *Nenroreport*, *8*, 3029–3037.

Näätänen, R. (1992). *Attention and brain function*. Hillsdale, NJ: Erlbaum.

Nunez, P. (1990). Localization of brain activity with electroencephalography. In S. Sato (Ed.), *Magnetoencephalography* (pp. 39–65). New York: Raven Press.

Opitz, B., Mecklinger, A., Friederici, A. D., & von Cramon, D. Y. (1998). The functional neuroanatomy of novelty processing: Integrating ERP and fMRI results. Manuscript submitted for publication.

Paavilainen, P., Alho, K., Reinikainen, K., Sams, M., & Näätänen, R. (1991). Right-hemisphere dominance of different mismatch negativities. *Electroencephalography and Clinical Neurophysiology*, *78*, 466–479.

Rolls, E., Thorpe, S., & Maddison, S. (1983). Responses of striatal neurons in the behaving monkey: I. Head of the caudate nucleus. *Behavioural Brain Research*, *7*, 179–210.

Scherg, M., Vajsar, J., & Picton, T. (1989). A source analysis of the late human auditory evoked potentials. *Journal of Cognitive Neuroscience*, *1*, 336–355.

Schröger, E. (1997). On the detection of auditory deviations: A preattentive activation model. *Psychophysiology*, *34*, 245–257.

Talairach, J., & Tournoux, P. (1988). *Co-Planar stereotaxis atlas of the human brain*. New York: Thieme.

Tarkka, I., Stokić, D., Basile, L., & Papanicolaou, A. (1995). Electric source localization of the auditory P300 agrees with magnetic source localization. *Electroencephalography and Clinical Neurophysiology*, *96*, 538–545.